Effective Integration of BCS with the IMSA to Enhance the Microwave Imaging of Sparse Objects Under the Born Approximation

N. Anselmi, L. Poli, G. Oliveri, and A. Massa

Abstract

In this work, the microwave imaging of sparse scatterers under the first order Born approximation is dealt with. Towards this end, an innovative Bayesian compressive sensing (*BCS*) methodology is derived and implemented in order to combine the well-known regularization capabilities of *CS* solvers with the progressively acquired information about the imaged scenario through the iterative multi-scaling approach (*IMSA*).
Selected numerical results are presented in order to verify the effectiveness of the proposed *IMSA-BCS* technique, as well as to compare it against competitive state-of-the-art approaches.

1 Numerical Results

1.1 E-shaped Object, $\ell = 1.5\lambda$

Test Case Description

Direct solver:

- Side of the investigation domain: $L = 6.0\lambda$
- Cubic domain divided in $\sqrt{D} \times \sqrt{D}$ cells
- Number of cells for the direct solver: $D = 1600$ (discretization $= \lambda/10$)

Investigation domain:

- Cubic domain divided in $\sqrt{N} \times \sqrt{N}$ cells
- Number of cells for the inversion:
  - First Step IMSA: $N^{(1)} = 100$ (discretization $= \lambda/10$)
  - Following Steps IMSA: $N^{(i)}$ not fixed, defined according to the estimated RoI $\mathcal{D}^{(i)}$

Measurement domain:

- Total number of measurements: $M = 60$
- Measurement points placed on circles of radius $\rho = 4.5\lambda$

Sources:

- Plane waves
- Number of views: $V = 60$; $\theta_{inc}^{v} = 0^\circ + (v-1) \times (360/V)$
- Amplitude: $A = 1.0$
- Frequency: $F = 300$ MHz ($\lambda = 1$)

Background:

- $\varepsilon_r = 1.0$
- $\sigma = 0$ [S/m]

Scatterer

- E-shaped object, $\ell = 1.5\lambda$
- $\varepsilon_r \in \{1.01, 1.02, 1.04, 1.05, 1.06, 1.08, 1.10, 1.15, 1.20\}$
- $\sigma = 0$ [S/m]

1.1.1 E-shaped Object, $\ell = 1.5\lambda$, $\tau = 0.02$ - $IMSA-BCS$ vs. $TVCS$ vs. BP reconstructed profiles

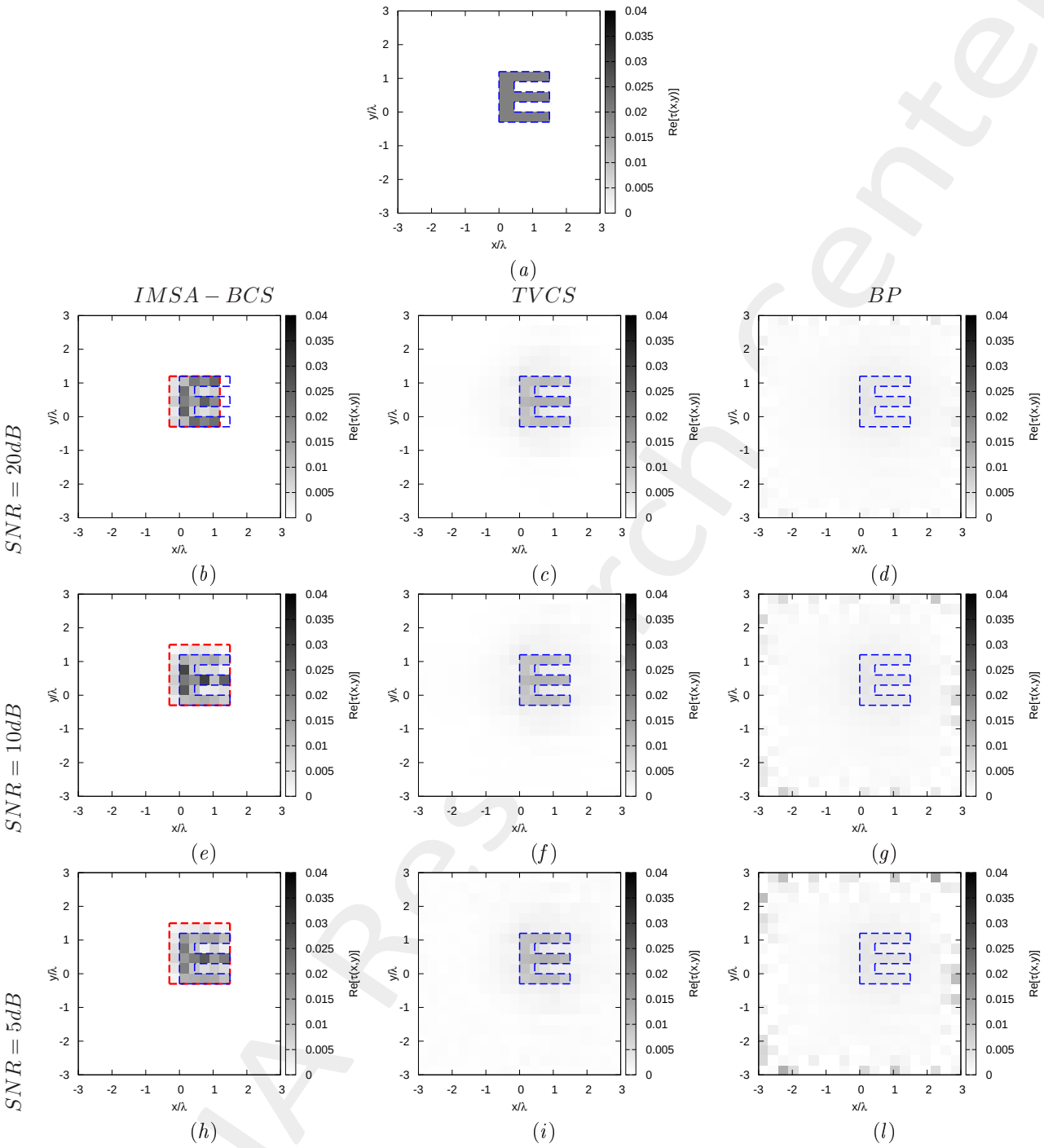

Figure 1: *E-shaped Object*, $\ell = 1.5\lambda$, $\tau = 0.02$ - *IMSA-BCS vs. TVCS vs. BP* - (a) Actual profile, $(b)(e)(h)$ $IMSA-BCS$, $(c)(f)(i)$ $TVCS$ and $(d)(g)(l)$ BP reconstructed profiles for $(b)(c)(d)$ $SNR = 20$ [dB], $(e)(f)(g)$ $SNR = 10$ [dB] and $(h)(i)(l)$ $SNR = 5$ [dB].

	$SNR = 50dB$		
	$IMSA-BCS$	$TVCS$	BP
ξ_{tot}	5.12×10^{-4}	9.10×10^{-4}	1.53×10^{-3}
ξ_{int}	7.76×10^{-3}	9.71×10^{-3}	1.57×10^{-2}
ξ_{ext}	1.71×10^{-4}	4.95×10^{-4}	8.64×10^{-4}
	$SNR = 20dB$		
	$IMSA-BCS$	$TVCS$	BP
ξ_{tot}	4.53×10^{-4}	9.17×10^{-4}	1.65×10^{-3}
ξ_{int}	6.70×10^{-3}	9.64×10^{-3}	1.57×10^{-2}
ξ_{ext}	1.56×10^{-4}	5.06×10^{-4}	9.27×10^{-4}
	$SNR = 10dB$		
	$IMSA-BCS$	$TVCS$	BP
ξ_{tot}	5.53×10^{-4}	1.00×10^{-3}	2.14×10^{-3}
ξ_{int}	8.04×10^{-3}	9.94×10^{-3}	1.57×10^{-2}
ξ_{ext}	1.99×10^{-4}	5.81×10^{-4}	1.25×10^{-3}
	$SNR = 5dB$		
	$IMSA-BCS$	$TVCS$	BP
ξ_{tot}	4.37×10^{-4}	1.18×10^{-3}	2.74×10^{-3}
ξ_{int}	5.40×10^{-3}	9.96×10^{-3}	1.57×10^{-2}
ξ_{ext}	2.01×10^{-4}	7.69×10^{-4}	1.68×10^{-3}

Table I: *E-shaped Object*, $\ell = 1.5\lambda$, $\tau = 0.02$ - *IMSA-BCS vs. TVCS vs. BP* - Reconstruction errors: total (ξ_{tot}), internal (ξ_{int}) and external (ξ_{ext}) errors.

1.1.2 E-shaped Object, $\ell = 1.5\lambda$, $\tau = 0.05$ - $IMSA-BCS$ vs. $TVCS$ vs. BP reconstructed profiles

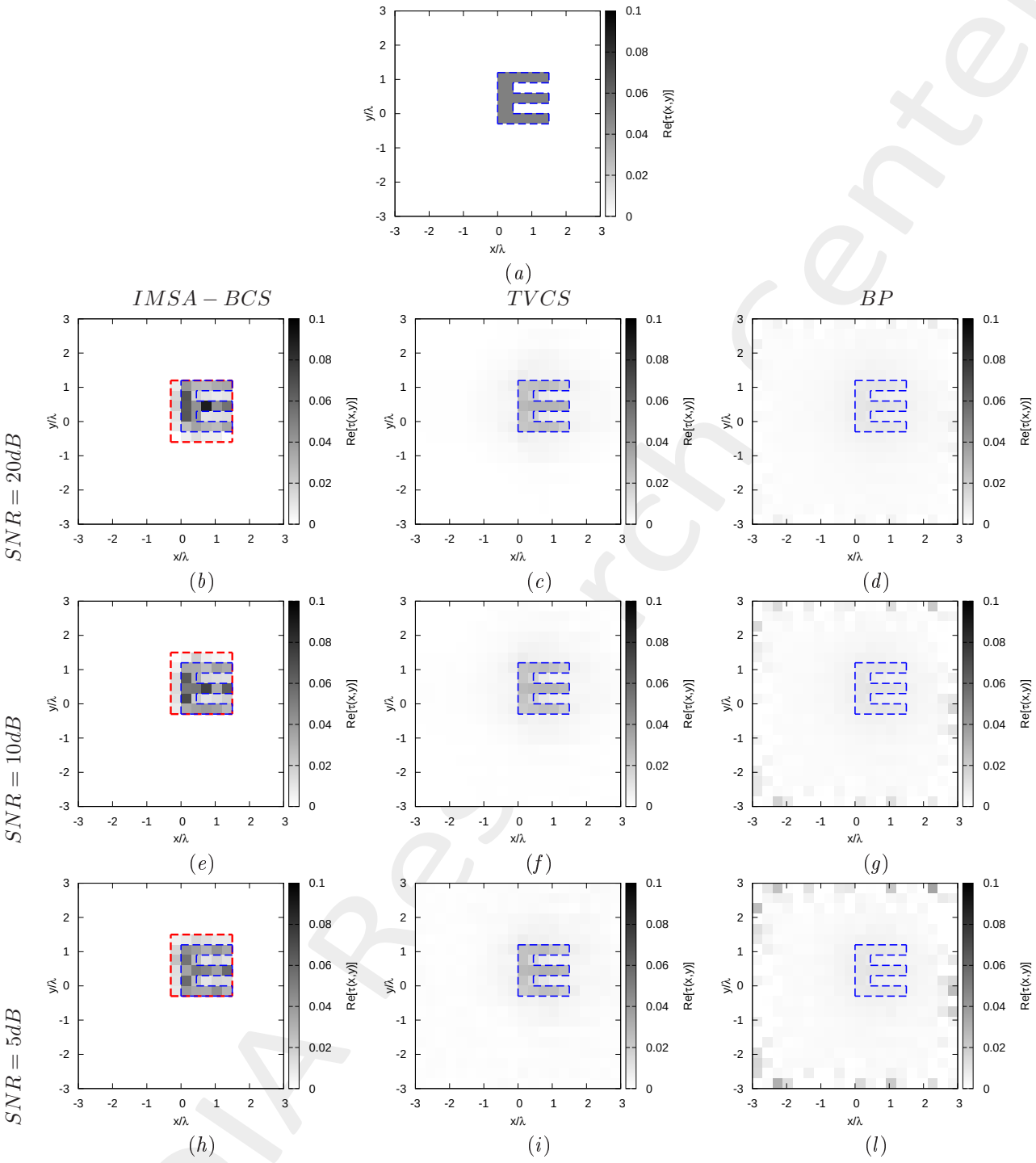

Figure 2: *E-shaped Object*, $\ell = 1.5\lambda$, $\tau = 0.05$ - *IMSA-BCS vs. TVCS vs. BP* - (a) Actual profile, $(b)(e)(h)$ $IMSA-BCS$, $(c)(f)(i)$ $TVCS$ and $(d)(g)(l)$ BP reconstructed profiles for $(b)(c)(d)$ $SNR = 20$ [dB], $(e)(f)(g)$ $SNR = 10$ [dB] and $(h)(i)(l)$ $SNR = 5$ [dB].

	$SNR = 50dB$		
	$IMSA-BCS$	$TVCS$	BP
ξ_{tot}	1.18×10^{-3}	2.29×10^{-3}	3.78×10^{-3}
ξ_{int}	1.54×10^{-2}	2.38×10^{-2}	3.82×10^{-2}
ξ_{ext}	4.92×10^{-4}	1.27×10^{-3}	2.15×10^{-3}
	$SNR = 20dB$		
	$IMSA-BCS$	$TVCS$	BP
ξ_{tot}	1.25×10^{-3}	2.30×10^{-3}	4.09×10^{-3}
ξ_{int}	1.64×10^{-2}	2.41×10^{-2}	3.82×10^{-2}
ξ_{ext}	5.15×10^{-4}	1.27×10^{-3}	2.31×10^{-3}
	$SNR = 10dB$		
	$IMSA-BCS$	$TVCS$	BP
ξ_{tot}	1.20×10^{-3}	2.55×10^{-3}	5.29×10^{-3}
ξ_{int}	1.52×10^{-2}	2.49×10^{-2}	3.82×10^{-2}
ξ_{ext}	5.25×10^{-4}	1.50×10^{-3}	3.12×10^{-3}
	$SNR = 5dB$		
	$IMSA-BCS$	$TVCS$	BP
ξ_{tot}	1.14×10^{-3}	2.91×10^{-3}	6.80×10^{-3}
ξ_{int}	1.10×10^{-2}	2.46×10^{-2}	3.83×10^{-2}
ξ_{ext}	6.34×10^{-4}	1.88×10^{-3}	4.18×10^{-3}

Table II: *E-shaped Object*, $\ell = 1.5\lambda$, $\tau = 0.05$ - *IMSA-BCS vs. TVCS vs. BP* - Reconstruction errors: total (ξ_{tot}), internal (ξ_{int}) and external (ξ_{ext}) errors.

1.1.3 E-shaped Object, $\ell = 1.5\lambda$, $\tau = 0.15$ - $IMSA-BCS$ vs. $TVCS$ vs. BP reconstructed profiles

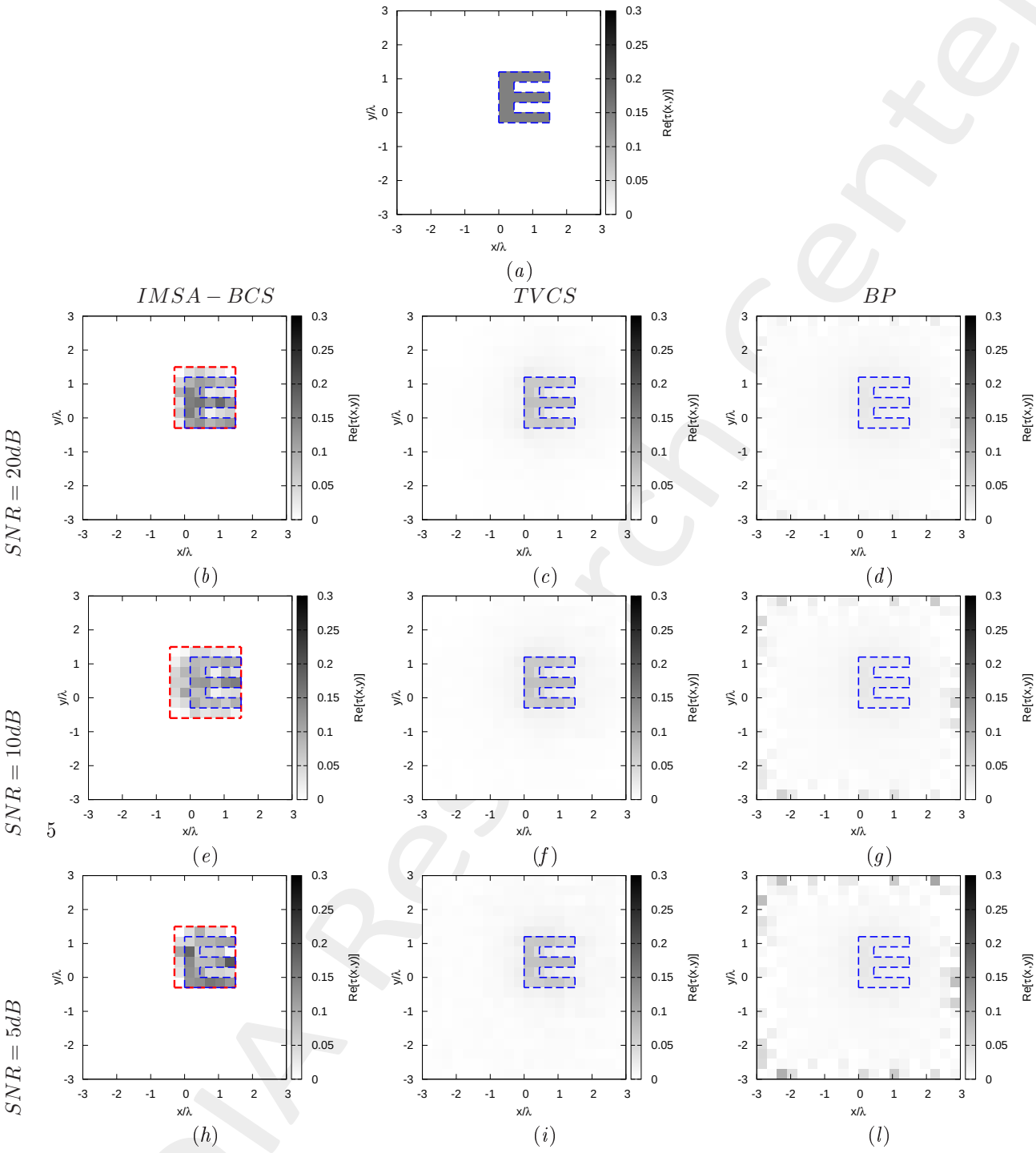

Figure 3: *E-shaped Object*, $\ell = 1.5\lambda$, $\tau = 0.15$ - *IMSA-BCS vs. TVCS vs. BP* - (a) Actual profile, $(b)(e)(h)$ $IMSA-BCS$, $(c)(f)(i)$ $TVCS$ and $(d)(g)(l)$ BP reconstructed profiles for $(b)(c)(d)$ $SNR = 20$ [dB], $(e)(f)(g)$ $SNR = 10$ [dB] and $(h)(i)(l)$ $SNR = 5$ [dB].

	$SNR = 50dB$		
	$IMSA-BCS$	$TVCS$	BP
ξ_{tot}	4.03×10^{-3}	7.41×10^{-3}	1.09×10^{-2}
ξ_{int}	4.09×10^{-2}	7.25×10^{-2}	1.06×10^{-1}
ξ_{ext}	1.78×10^{-3}	4.34×10^{-3}	6.24×10^{-3}
	$SNR = 20dB$		
	$IMSA-BCS$	$TVCS$	BP
ξ_{tot}	3.80×10^{-3}	7.50×10^{-3}	1.18×10^{-2}
ξ_{int}	3.13×10^{-2}	7.48×10^{-2}	1.06×10^{-1}
ξ_{ext}	1.89×10^{-3}	4.33×10^{-3}	6.70×10^{-3}
	$SNR = 10dB$		
	$IMSA-BCS$	$TVCS$	BP
ξ_{tot}	5.61×10^{-3}	8.12×10^{-3}	1.53×10^{-2}
ξ_{int}	4.88×10^{-2}	7.52×10^{-2}	1.06×10^{-1}
ξ_{ext}	3.11×10^{-3}	4.96×10^{-3}	9.09×10^{-3}
	$SNR = 5dB$		
	$IMSA-BCS$	$TVCS$	BP
ξ_{tot}	4.67×10^{-3}	9.24×10^{-3}	1.97×10^{-2}
ξ_{int}	3.57×10^{-2}	7.55×10^{-2}	1.06×10^{-1}
ξ_{ext}	2.18×10^{-3}	6.11×10^{-3}	1.21×10^{-2}

Table III: *E-shaped Object*, $\ell = 1.5\lambda$, $\tau = 0.15$ - *IMSA-BCS vs. TVCS vs. BP* - Reconstruction errors: total (ξ_{tot}), internal (ξ_{int}) and external (ξ_{ext}) errors.

1.1.4 E-shaped Object, $\ell = 1.5\lambda$, $\tau = 0.20$ - $IMSA-BCS$ vs. $TVCS$ vs. BP reconstructed profiles

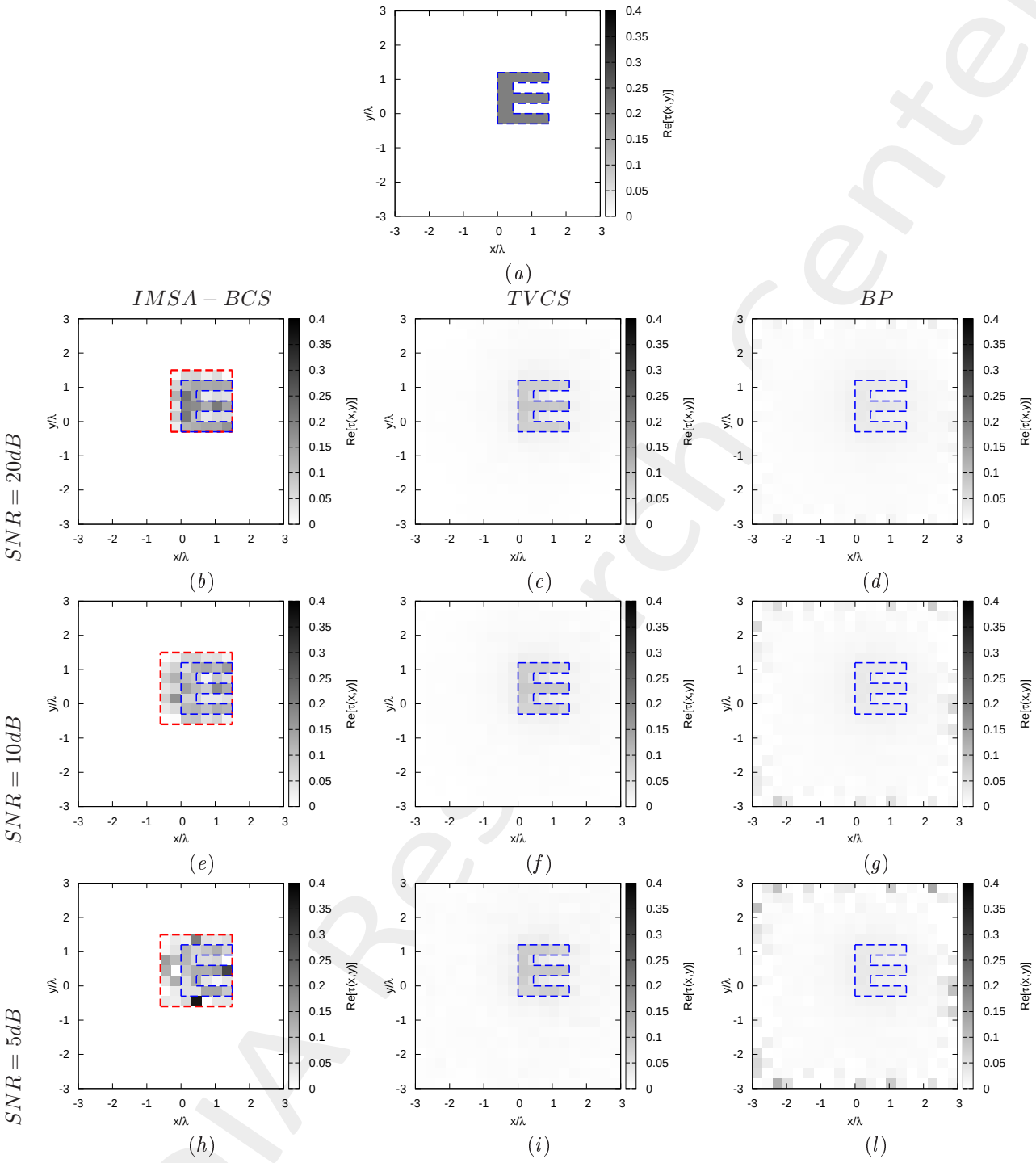

Figure 4: *E-shaped Object*, $\ell = 1.5\lambda$, $\tau = 0.20$ - *IMSA-BCS vs. TVCS vs. BP* - (a) Actual profile, $(b)(e)(h)$ $IMSA-BCS$, $(c)(f)(i)$ $TVCS$ and $(d)(g)(l)$ BP reconstructed profiles for $(b)(c)(d)$ $SNR = 20$ [dB], $(e)(f)(g)$ $SNR = 10$ [dB] and $(h)(i)(l)$ $SNR = 5$ [dB].

	$SNR = 50dB$		
	$IMSA-BCS$	$TVCS$	BP
ξ_{tot}	5.14×10^{-3}	1.02×10^{-2}	1.43×10^{-2}
ξ_{int}	4.33×10^{-2}	1.01×10^{-1}	1.37×10^{-1}
ξ_{ext}	2.23×10^{-3}	5.96×10^{-3}	8.07×10^{-3}
	$SNR = 20dB$		
	$IMSA-BCS$	$TVCS$	BP
ξ_{tot}	5.42×10^{-3}	1.04×10^{-2}	1.54×10^{-2}
ξ_{int}	4.39×10^{-2}	1.01×10^{-1}	1.37×10^{-1}
ξ_{ext}	2.52×10^{-3}	6.11×10^{-3}	8.69×10^{-3}
	$SNR = 10dB$		
	$IMSA-BCS$	$TVCS$	BP
ξ_{tot}	8.31×10^{-3}	1.12×10^{-2}	2.00×10^{-2}
ξ_{int}	7.27×10^{-2}	1.03×10^{-1}	1.37×10^{-1}
ξ_{ext}	4.44×10^{-3}	6.89×10^{-3}	1.18×10^{-2}
	$SNR = 5dB$		
	$IMSA-BCS$	$TVCS$	BP
ξ_{tot}	1.15×10^{-2}	1.27×10^{-2}	2.58×10^{-2}
ξ_{int}	8.38×10^{-2}	1.03×10^{-1}	1.37×10^{-1}
ξ_{ext}	5.40×10^{-3}	8.46×10^{-3}	1.59×10^{-2}

Table IV: *E-shaped Object*, $\ell = 1.5\lambda$, $\tau = 0.20$ - *IMSA-BCS vs. TVCS vs. BP* - Reconstruction errors: total (ξ_{tot}), internal (ξ_{int}) and external (ξ_{ext}) errors.

1.1.5 E-shaped Object, $\ell = 1.5\lambda$ - $IMSA-BCS$ vs. $TVCS$ vs. BP errors resume vs. τ

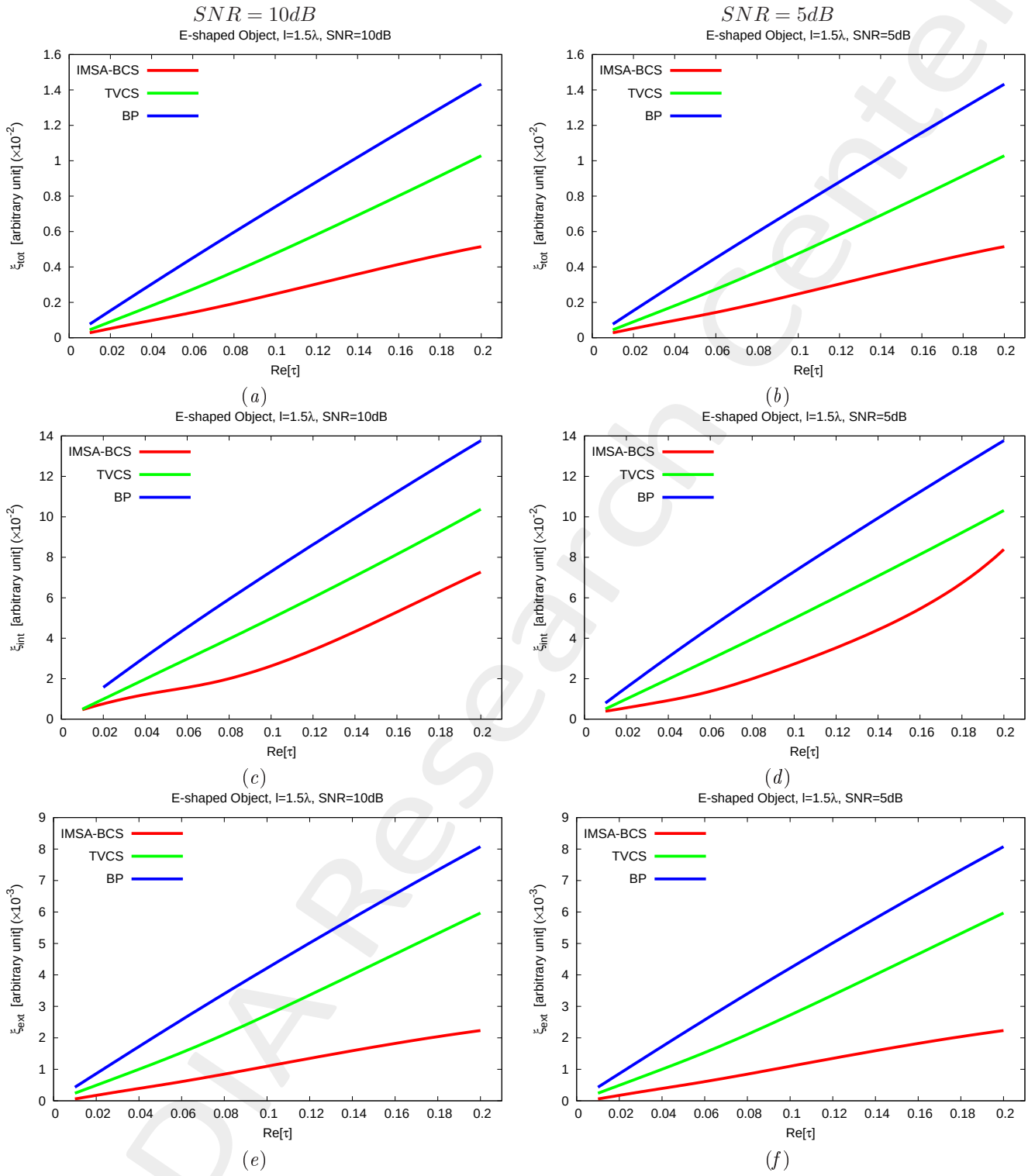

Figure 5: *E-shaped Object*, $\ell = 1.5\lambda$ - Reconstruction errors vs. τ: (a) total error, (b) internal error and (c) external error. Reconstruction errors vs. τ: $(a)(b)$ total error, $(c)(d)$ internal error and $(e)(f)$ external error for $(a)(c)(e)$ $SNR = 10dB$ and $(b)(d)(f)$ $SNR = 5dB$.

1.2 Rhombus, $D = 1.5\lambda$

Test Case Description

Direct solver:

- Side of the investigation domain: $L = 6.0\lambda$
- Cubic domain divided in $\sqrt{D} \times \sqrt{D}$ cells
- Number of cells for the direct solver: $D = 1600$ (discretization = $\lambda/10$)

Investigation domain:

- Cubic domain divided in $\sqrt{N} \times \sqrt{N}$ cells
- Number of cells for the inversion:
  - First Step IMSA: $N^{(1)} = 100$ (discretization = $\lambda/10$)
  - Following Steps IMSA: $N^{(i)}$ not fixed, defined according to the estimated RoI $\mathcal{D}^{(i)}$

Measurement domain:

- Total number of measurements: $M = 60$
- Measurement points placed on circles of radius $\rho = 4.5\lambda$

Sources:

- Plane waves
- Number of views: $V = 60$; $\theta_{inc}^{v} = 0^\circ + (v-1) \times (360/V)$
- Amplitude: $A = 1.0$
- Frequency: $F = 300$ MHz ($\lambda = 1$)

Background:

- $\varepsilon_r = 1.0$
- $\sigma = 0$ [S/m]

Scatterer

- Rhombus, $D = 1.5\lambda$
- $\varepsilon_r \in \{1.01,\ 1.02,\ 1.04, 1.05,\ 1.06,\ 1.08,\ 1.10,\ 1.15,\ 1.20\}$
- $\sigma = 0$ [S/m]

1.2.1 Rhombus, $D = 1.5\lambda$, $\tau = 0.02$ - $IMSA-BCS$ vs. $TVCS$ vs. BP reconstructed profiles

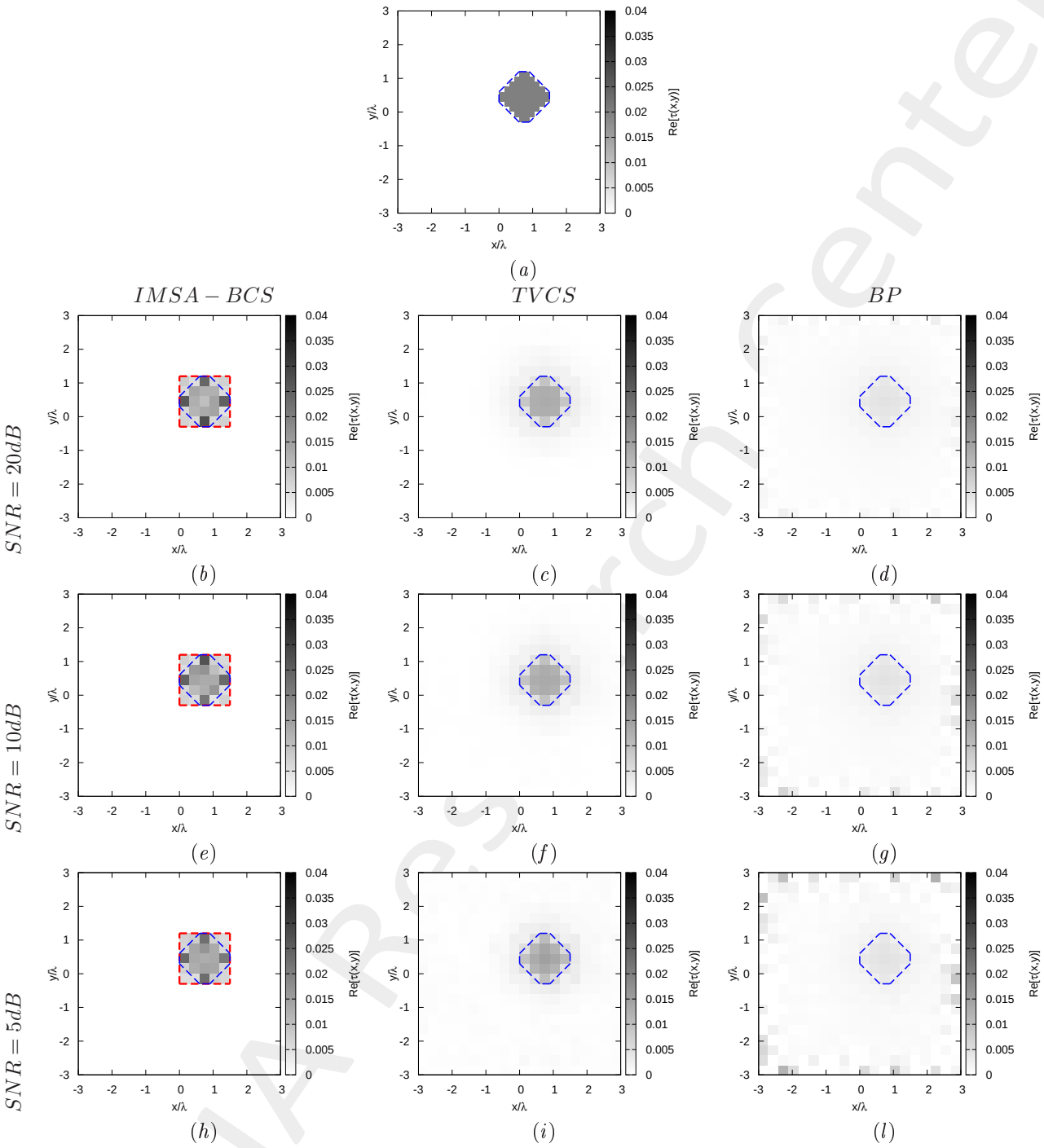

Figure 6: *Rhombus*, $D = 1.5\lambda$, $\tau = 0.02$ - *IMSA-BCS vs. TVCS vs. BP* - (a) Actual profile, $(b)(e)(h)$ $IMSA-BCS$, $(c)(f)(i)$ $TVCS$ and $(d)(g)(l)$ BP reconstructed profiles for $(b)(c)(d)$ $SNR = 20$ [dB], $(e)(f)(g)$ $SNR = 10$ [dB] and $(h)(i)(l)$ $SNR = 5$ [dB].

	$SNR = 50dB$		
	$IMSA-BCS$	$TVCS$	BP
ξ_{tot}	4.48×10^{-4}	7.59×10^{-4}	1.28×10^{-3}
ξ_{int}	7.80×10^{-3}	9.47×10^{-3}	1.58×10^{-2}
ξ_{ext}	1.62×10^{-4}	4.19×10^{-4}	7.20×10^{-4}
	$SNR = 20dB$		
	$IMSA-BCS$	$TVCS$	BP
ξ_{tot}	4.44×10^{-4}	7.59×10^{-4}	1.40×10^{-3}
ξ_{int}	7.59×10^{-3}	9.17×10^{-3}	1.58×10^{-2}
ξ_{ext}	1.66×10^{-4}	4.31×10^{-4}	7.82×10^{-4}
	$SNR = 10dB$		
	$IMSA-BCS$	$TVCS$	BP
ξ_{tot}	4.04×10^{-4}	8.36×10^{-4}	1.85×10^{-3}
ξ_{int}	6.67×10^{-3}	9.00×10^{-3}	1.58×10^{-2}
ξ_{ext}	1.59×10^{-4}	5.18×10^{-4}	1.09×10^{-3}
	$SNR = 5dB$		
	$IMSA-BCS$	$TVCS$	BP
ξ_{tot}	3.88×10^{-4}	9.70×10^{-4}	2.42×10^{-3}
ξ_{int}	6.03×10^{-3}	8.61×10^{-3}	1.58×10^{-2}
ξ_{ext}	1.67×10^{-4}	6.72×10^{-4}	1.48×10^{-3}

Table V: *Rhombus*, $D = 1.5\lambda$, $\tau = 0.02$ - *IMSA-BCS vs. TVCS vs. BP* - Reconstruction errors: total (ξ_{tot}), internal (ξ_{int}) and external (ξ_{ext}) errors.

1.2.2 Rhombus, $D = 1.5\lambda$, $\tau = 0.05$ - $IMSA-BCS$ vs. $TVCS$ vs. BP reconstructed profiles

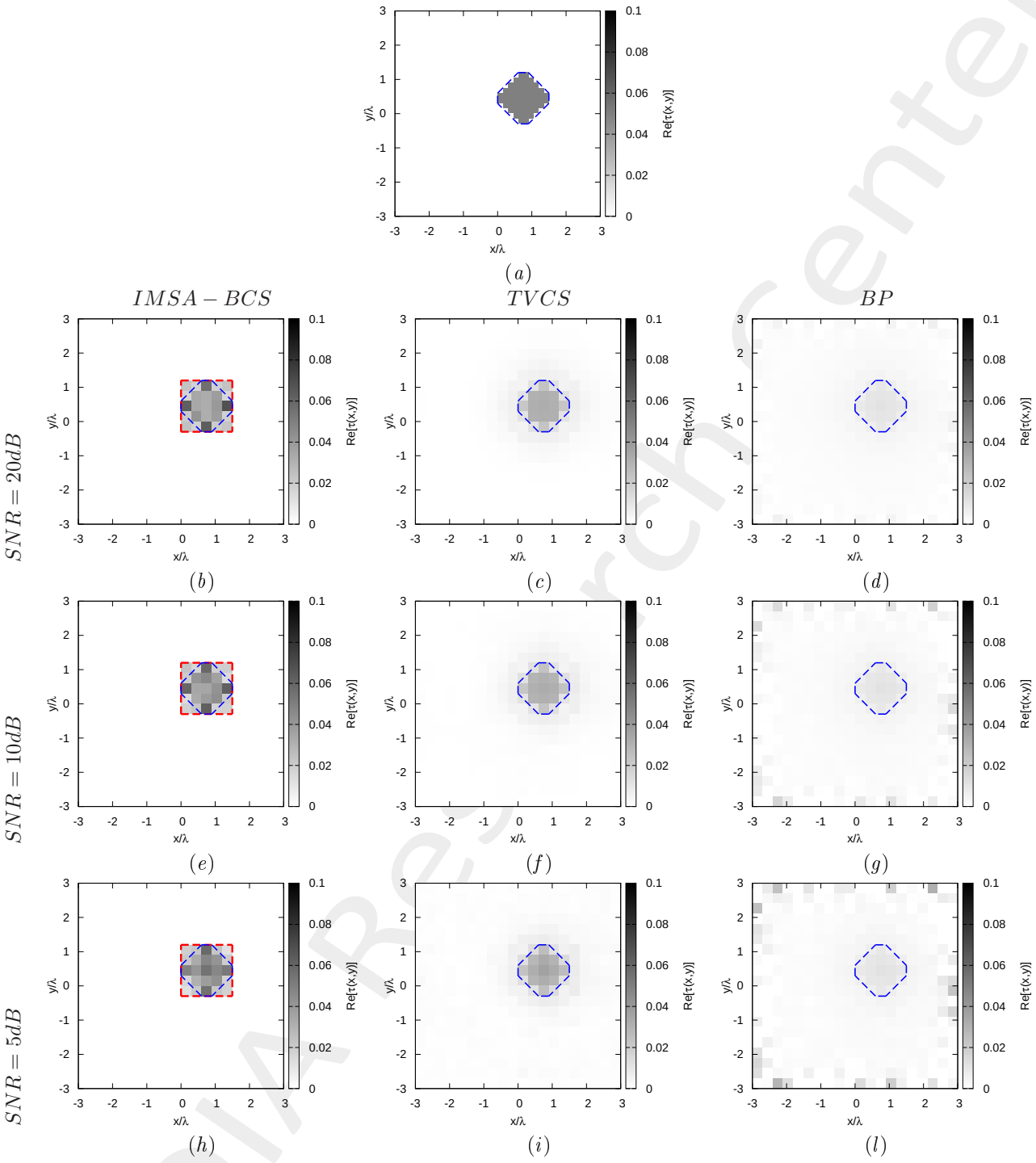

Figure 7: *Rhombus*, $D = 1.5\lambda$, $\tau = 0.05$ - *IMSA-BCS vs. TVCS vs. BP* - (a) Actual profile, $(b)(e)(h)$ $IMSA-BCS$, $(c)(f)(i)$ $TVCS$ and $(d)(g)(l)$ BP reconstructed profiles for $(b)(c)(d)$ $SNR = 20$ [dB], $(e)(f)(g)$ $SNR = 10$ [dB] and $(h)(i)(l)$ $SNR = 5$ [dB].

	$SNR = 50dB$		
	$IMSA-BCS$	$TVCS$	BP
ξ_{tot}	1.12×10^{-3}	1.91×10^{-3}	2.55×10^{-3}
ξ_{int}	1.65×10^{-2}	2.28×10^{-2}	3.11×10^{-2}
ξ_{ext}	5.13×10^{-4}	1.09×10^{-3}	1.43×10^{-3}
	$SNR = 20dB$		
	$IMSA-BCS$	$TVCS$	BP
ξ_{tot}	1.09×10^{-3}	1.91×10^{-3}	2.79×10^{-3}
ξ_{int}	1.53×10^{-2}	2.25×10^{-2}	3.11×10^{-2}
ξ_{ext}	5.27×10^{-4}	1.10×10^{-3}	1.56×10^{-3}
	$SNR = 10dB$		
	$IMSA-BCS$	$TVCS$	BP
ξ_{tot}	9.67×10^{-4}	2.12×10^{-3}	3.69×10^{-3}
ξ_{int}	1.30×10^{-2}	2.26×10^{-2}	3.11×10^{-2}
ξ_{ext}	4.81×10^{-4}	1.32×10^{-3}	2.17×10^{-3}
	$SNR = 5dB$		
	$IMSA-BCS$	$TVCS$	BP
ξ_{tot}	8.71×10^{-4}	2.44×10^{-3}	4.81×10^{-3}
ξ_{int}	1.01×10^{-2}	2.16×10^{-2}	3.11×10^{-2}
ξ_{ext}	4.74×10^{-4}	1.69×10^{-3}	2.96×10^{-3}

Table VI: *Rhombus*, $D = 1.5\lambda$, $\tau = 0.05$ - *IMSA-BCS vs. TVCS vs. BP* - Reconstruction errors: total (ξ_{tot}), internal (ξ_{int}) and external (ξ_{ext}) errors.

1.2.3 Rhombus, $D = 1.5\lambda$, $\tau = 0.10$ - $IMSA - BCS$ vs. $TVCS$ vs. BP reconstructed profiles

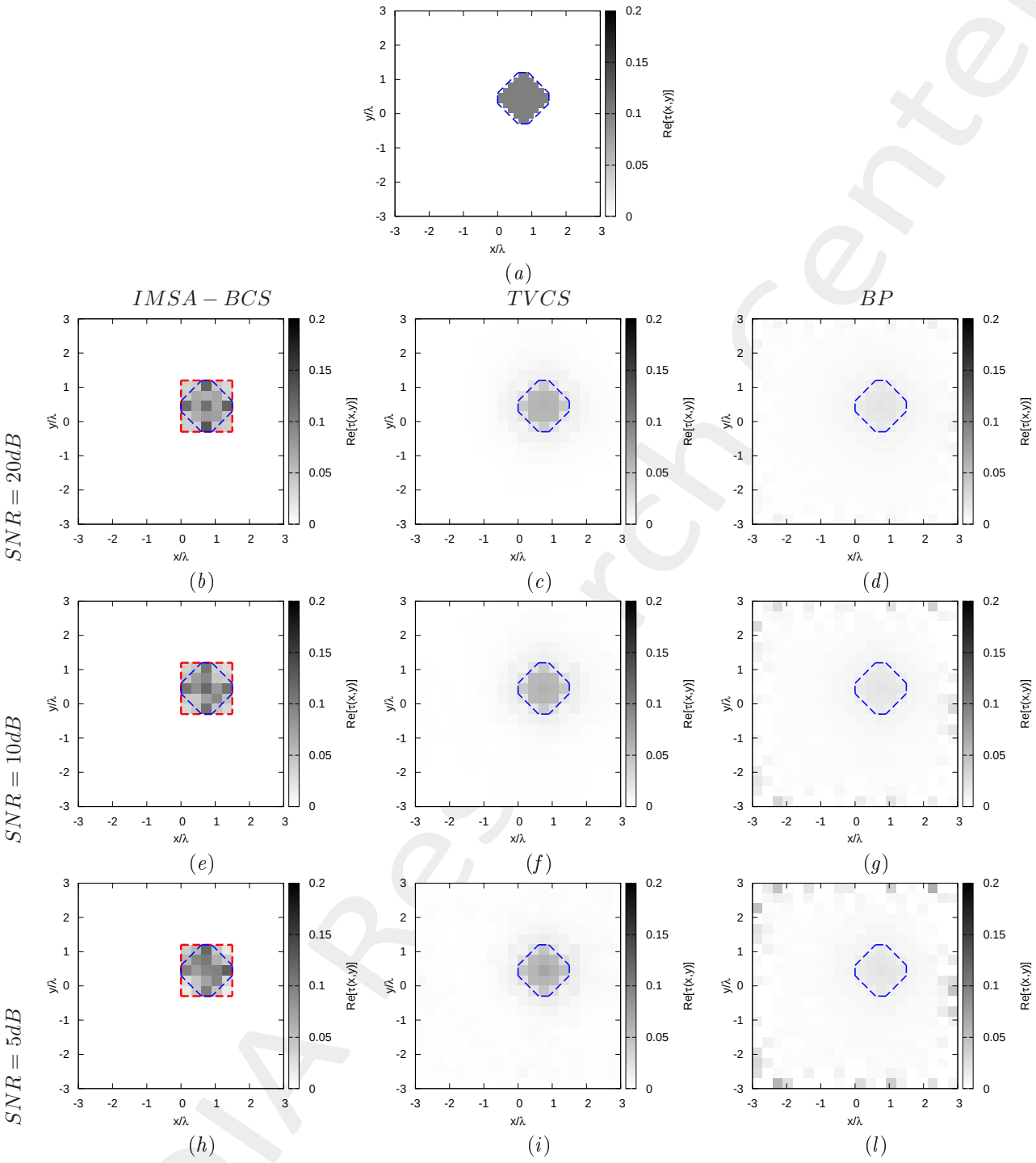

Figure 8: *Rhombus*, $D = 1.5\lambda$, $\tau = 0.02$ - *IMSA-BCS vs. TVCS vs. BP* - (a) Actual profile, $(b)(e)(h)$ $IMSA-BCS$, $(c)(f)(i)$ $TVCS$ and $(d)(g)(l)$ BP reconstructed profiles for $(b)(c)(d)$ $SNR = 20$ [dB], $(e)(f)(g)$ $SNR = 10$ [dB] and $(h)(i)(l)$ $SNR = 5$ [dB].

	$SNR = 50dB$		
	$IMSA-BCS$	$TVCS$	BP
ξ_{tot}	2.10×10^{-3}	3.89×10^{-3}	6.23×10^{-3}
ξ_{int}	2.72×10^{-2}	4.62×10^{-2}	7.40×10^{-2}
ξ_{ext}	9.86×10^{-4}	2.24×10^{-3}	3.53×10^{-3}
	$SNR = 20dB$		
	$IMSA-BCS$	$TVCS$	BP
ξ_{tot}	2.18×10^{-3}	3.96×10^{-3}	6.82×10^{-3}
ξ_{int}	2.81×10^{-2}	4.66×10^{-2}	7.40×10^{-2}
ξ_{ext}	1.01×10^{-3}	2.29×10^{-3}	3.84×10^{-3}
	$SNR = 10dB$		
	$IMSA-BCS$	$TVCS$	BP
ξ_{tot}	2.05×10^{-3}	4.34×10^{-3}	9.04×10^{-3}
ξ_{int}	2.29×10^{-2}	4.67×10^{-2}	7.40×10^{-2}
ξ_{ext}	1.02×10^{-3}	2.69×10^{-3}	5.37×10^{-3}
	$SNR = 5dB$		
	$IMSA-BCS$	$TVCS$	BP
ξ_{tot}	1.88×10^{-3}	5.01×10^{-3}	1.18×10^{-2}
ξ_{int}	1.95×10^{-2}	4.43×10^{-2}	7.40×10^{-2}
ξ_{ext}	9.40×10^{-4}	3.48×10^{-3}	7.32×10^{-3}

Table VII: *Rhombus*, $D = 1.5\lambda$, $\tau = 0.10$ - *IMSA-BCS vs. TVCS vs. BP* - Reconstruction errors: total (ξ_{tot}), internal (ξ_{int}) and external (ξ_{ext}) errors.

1.2.4 Rhombus, $D = 1.5\lambda$, $\tau = 0.15$ - $IMSA-BCS$ vs. $TVCS$ vs. BP reconstructed profiles

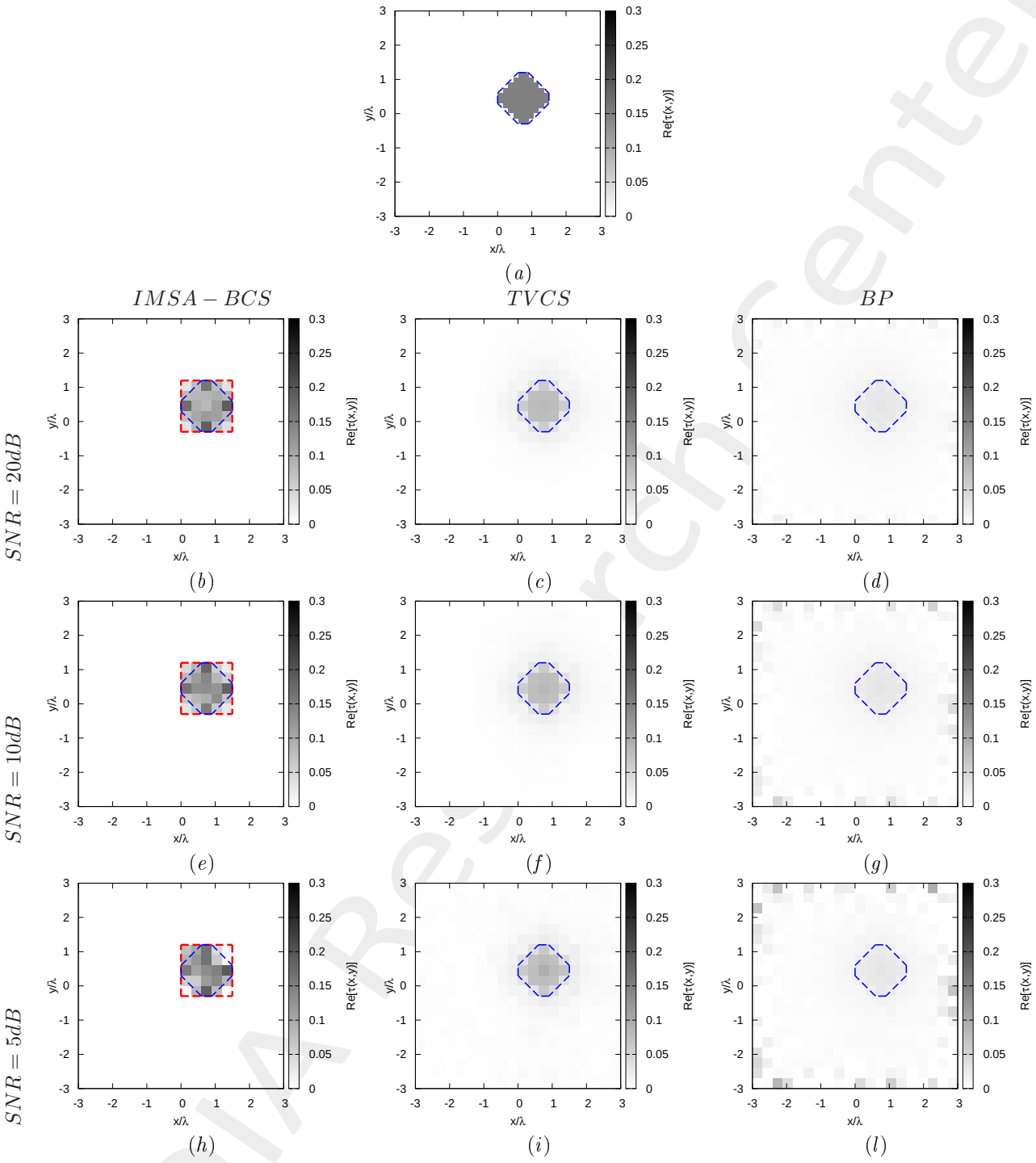

Figure 9: *Rhombus*, $D = 1.5\lambda$, $\tau = 0.15$ - *IMSA-BCS vs. TVCS vs. BP* - (a) Actual profile, $(b)(e)(h)$ $IMSA-BCS$, $(c)(f)(i)$ $TVCS$ and $(d)(g)(l)$ BP reconstructed profiles for $(b)(c)(d)$ $SNR = 20$ [dB], $(e)(f)(g)$ $SNR = 10$ [dB] and $(h)(i)(l)$ $SNR = 5$ [dB].

	$SNR = 50dB$		
	$IMSA-BCS$	$TVCS$	BP
ξ_{tot}	3.51×10^{-3}	6.20×10^{-3}	9.17×10^{-3}
ξ_{int}	4.27×10^{-2}	7.17×10^{-2}	1.07×10^{-1}
ξ_{ext}	1.52×10^{-3}	3.64×10^{-3}	5.18×10^{-3}
	$SNR = 20dB$		
	$IMSA-BCS$	$TVCS$	BP
ξ_{tot}	3.53×10^{-3}	6.28×10^{-3}	1.00×10^{-2}
ξ_{int}	4.09×10^{-2}	7.20×10^{-2}	1.07×10^{-1}
ξ_{ext}	1.62×10^{-3}	3.71×10^{-3}	5.65×10^{-3}
	$SNR = 10dB$		
	$IMSA-BCS$	$TVCS$	BP
ξ_{tot}	3.06×10^{-3}	6.76×10^{-3}	1.33×10^{-2}
ξ_{int}	3.18×10^{-2}	7.19×10^{-2}	1.07×10^{-1}
ξ_{ext}	1.38×10^{-3}	4.22×10^{-3}	7.91×10^{-3}
	$SNR = 5dB$		
	$IMSA-BCS$	$TVCS$	BP
ξ_{tot}	3.39×10^{-3}	7.73×10^{-3}	1.74×10^{-2}
ξ_{int}	3.40×10^{-2}	6.94×10^{-2}	1.07×10^{-1}
ξ_{ext}	1.32×10^{-3}	5.33×10^{-3}	1.08×10^{-2}

Table VIII: *Rhombus*, $D = 1.5\lambda$, $\tau = 0.15$ - *IMSA-BCS vs. TVCS vs. BP* - Reconstruction errors: total (ξ_{tot}), internal (ξ_{int}) and external (ξ_{ext}) errors.

1.2.5 Rhombus, $D = 1.5\lambda$, $\tau = 0.20$ - $IMSA-BCS$ vs. $TVCS$ vs. BP reconstructed profiles

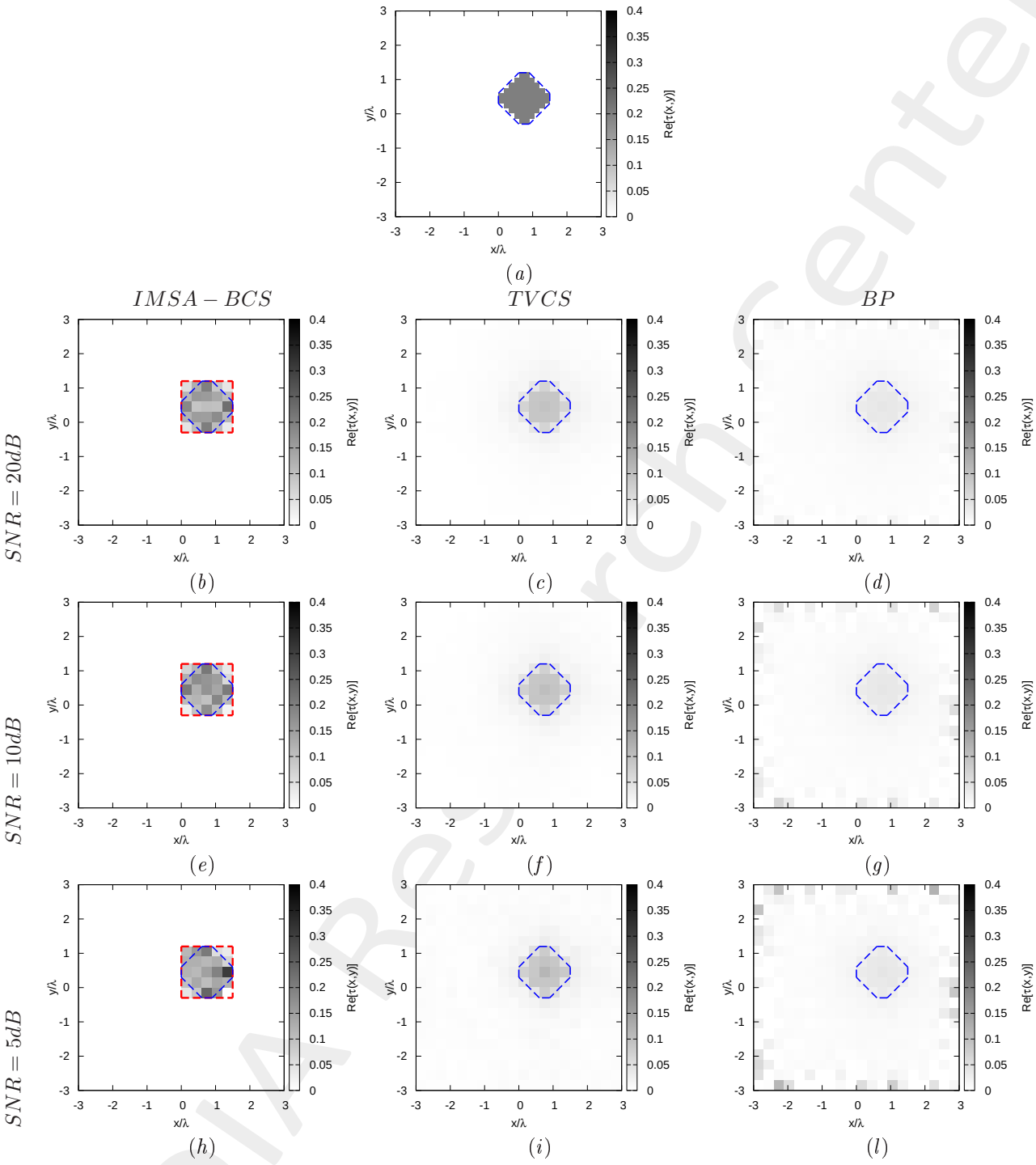

Figure 10: *Rhombus*, $D = 1.5\lambda$, $\tau = 0.20$ - *IMSA-BCS vs. TVCS vs. BP* - (a) Actual profile, $(b)(e)(h)$ $IMSA-BCS$, $(c)(f)(i)$ $TVCS$ and $(d)(g)(l)$ BP reconstructed profiles for $(b)(c)(d)$ $SNR = 20$ [dB], $(e)(f)(g)$ $SNR = 10$ [dB] and $(h)(i)(l)$ $SNR = 5$ [dB].

	$SNR = 50dB$		
	$IMSA-BCS$	$TVCS$	BP
ξ_{tot}	4.83×10^{-3}	8.84×10^{-3}	1.19×10^{-2}
ξ_{int}	4.18×10^{-2}	1.01×10^{-1}	1.38×10^{-1}
ξ_{ext}	2.16×10^{-3}	5.25×10^{-3}	6.69×10^{-3}
	$SNR = 20dB$		
	$IMSA-BCS$	$TVCS$	BP
ξ_{tot}	4.86×10^{-3}	8.86×10^{-3}	1.31×10^{-2}
ξ_{int}	4.42×10^{-2}	1.01×10^{-1}	1.38×10^{-1}
ξ_{ext}	2.13×10^{-3}	5.25×10^{-3}	7.31×10^{-3}
	$SNR = 10dB$		
	$IMSA-BCS$	$TVCS$	BP
ξ_{tot}	4.56×10^{-3}	9.40×10^{-3}	1.74×10^{-2}
ξ_{int}	3.97×10^{-2}	9.96×10^{-2}	1.38×10^{-1}
ξ_{ext}	1.95×10^{-3}	5.89×10^{-3}	1.03×10^{-2}
	$SNR = 5dB$		
	$IMSA-BCS$	$TVCS$	BP
ξ_{tot}	5.47×10^{-3}	1.07×10^{-2}	2.28×10^{-2}
ξ_{int}	5.71×10^{-2}	9.75×10^{-2}	1.38×10^{-1}
ξ_{ext}	2.22×10^{-3}	7.34×10^{-3}	1.41×10^{-2}

Table IX: *Rhombus*, $D = 1.5\lambda$, $\tau = 0.20$ - *IMSA-BCS vs. TVCS vs. BP* - Reconstruction errors: total (ξ_{tot}), internal (ξ_{int}) and external (ξ_{ext}) errors.

1.2.6 Rhombus, $D = 1.5\lambda$ - $IMSA - BCS$ vs. $TVCS$ vs. BP errors resume vs. τ

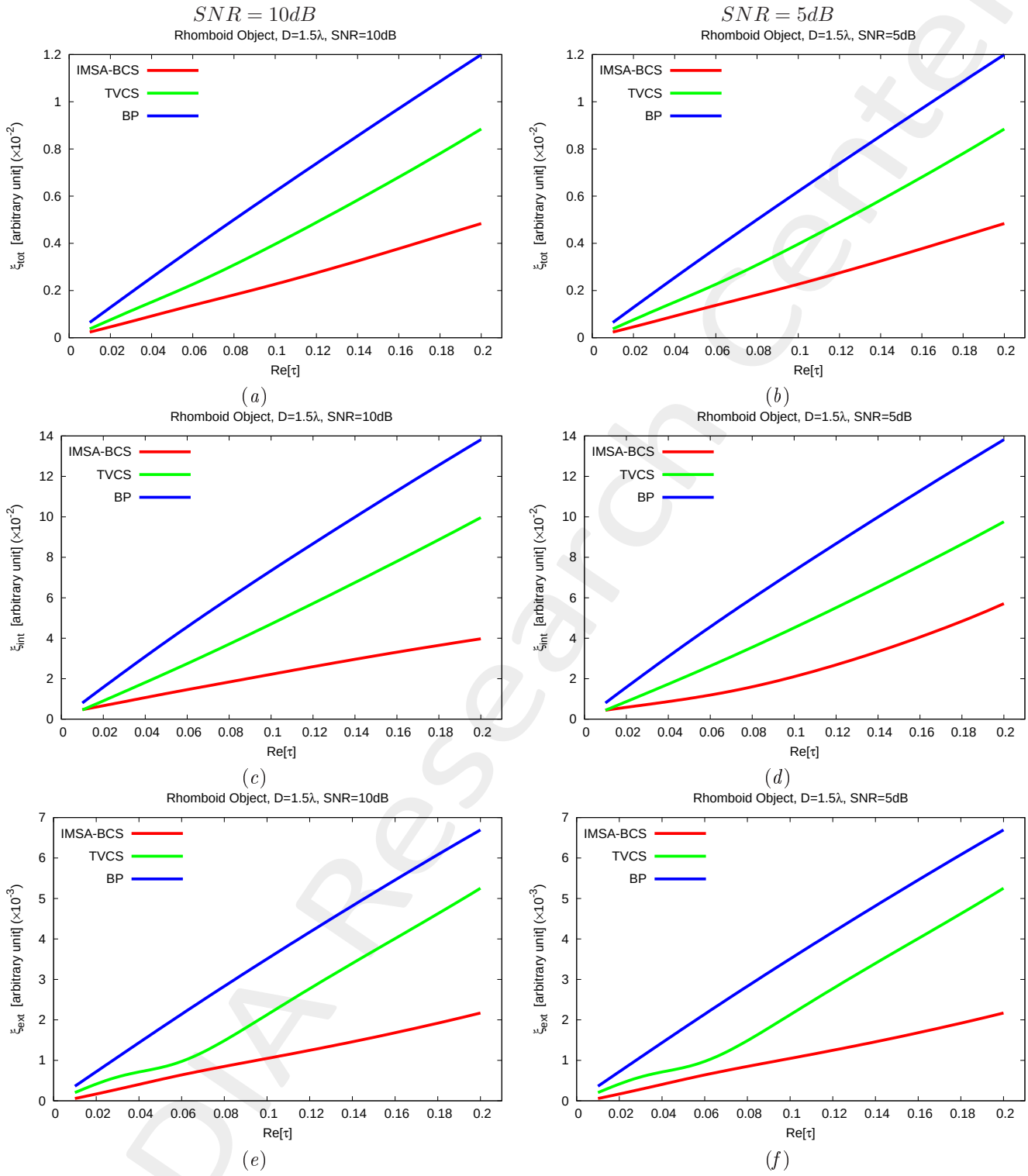

Figure 11: *Rhombus*, $D = 1.5\lambda$ - Reconstruction errors vs. τ: (a) total error, (b) internal error and (c) external error. Reconstruction errors vs. τ: $(a)(b)$ total error, $(c)(d)$ internal error and $(e)(f)$ external error for $(a)(c)(e)$ $SNR = 10dB$ and $(b)(d)(f)$ $SNR = 5dB$.

References

[1] M. Salucci, G. Oliveri, and A. Massa, "GPR prospecting through an inverse scattering frequency-hopping multi-focusing approach," *IEEE Trans. Geosci. Remote Sens.*, vol. 53, no. 12, pp. 6573-6592, Dec. 2015.

[2] M. Salucci, L. Poli, N. Anselmi, and A. Massa, "Multifrequency Particle Swarm Optimization for enhanced multiresolution GPR microwave imaging," *IEEE Trans. Geosci. Remote Sens.*, vol. 55, no. 3, pp. 1305-1317, Mar. 2017.

[3] M. Salucci, L. Poli, and A. Massa, "Advanced multi-frequency GPR data processing for non-linear deterministic imaging," *Signal Processing* - Special Issue on 'Advanced Ground-Penetrating Radar Signal-Processing Techniques,' vol. 132, pp. 306-318, Mar. 2017.

[4] N. Anselmi, G. Oliveri, M. Salucci, and A. Massa, "Wavelet-based compressive imaging of sparse targets," *IEEE Trans. Antennas Propag.*, vol. 63, no. 11, pp. 4889-4900, Nov. 2015.

[5] G. Oliveri, M. Salucci, N. Anselmi, and A. Massa, "Compressive sensing as applied to inverse problems for imaging: theory, applications, current trends, and open challenges," *IEEE Antennas Propag. Mag.* - Special Issue on "Electromagnetic Inverse Problems for Sensing and Imaging," vol. 59, no. 5, pp. 34-46, Oct. 2017.

[6] A. Massa, P. Rocca, and G. Oliveri, "Compressive sensing in electromagnetics - A review," *IEEE Antennas Propag. Mag.*, pp. 224-238, vol. 57, no. 1, Feb. 2015.

[7] N. Anselmi, L. Poli, G. Oliveri, and A. Massa, "Iterative multi-resolution bayesian CS for microwave imaging," *IEEE Trans. Antennas Propag.*, vol. 66, no. 7, pp. 3665-3677, Jul. 2018.

[8] N. Anselmi, G. Oliveri, M. A. Hannan, M. Salucci, and A. Massa, "Color compressive sensing imaging of arbitrary-shaped scatterers," *IEEE Trans. Microw. Theory Techn.*, vol. 65, no. 6, pp. 1986-1999, Jun. 2017.

[9] G. Oliveri, N. Anselmi, and A. Massa, "Compressive sensing imaging of non-sparse 2D scatterers by a total-variation approach within the Born approximation," *IEEE Trans. Antennas Propag.*, vol. 62, no. 10, pp. 5157-5170, Oct. 2014.

[10] L. Poli, G. Oliveri, and A. Massa, "Imaging sparse metallic cylinders through a local shape function Bayesian compressive sensing approach," *Journal of Optical Society of America A*, vol. 30, no. 6, pp. 1261-1272, 2013.

[11] L. Poli, G. Oliveri, F. Viani, and A. Massa, "MT-BCS-based microwave imaging approach through minimum-norm current expansion," *IEEE Trans. Antennas Propag.*, vol. 61, no. 9, pp. 4722-4732, Sep. 2013.

[12] F. Viani, L. Poli, G. Oliveri, F. Robol, and A. Massa, "Sparse scatterers imaging through approximated multitask compressive sensing strategies," *Microwave Opt. Technol. Lett.*, vol. 55, no. 7, pp. 1553-1558, Jul. 2013.

[13] L. Poli, G. Oliveri, P. Rocca, and A. Massa, "Bayesian compressive sensing approaches for the reconstruction of two-dimensional sparse scatterers under TE illumination," *IEEE Trans. Geosci. Remote Sens.*, vol. 51, no. 5, pp. 2920-2936, May 2013.

[14] L. Poli, G. Oliveri, and A. Massa, "Microwave imaging within the first-order Born approximation by means of the contrast-field Bayesian compressive sensing," *IEEE Trans. Antennas Propag.*, vol. 60, no. 6, pp. 2865-2879, Jun. 2012.

[15] G. Oliveri, L. Poli, P. Rocca, and A. Massa, "Bayesian compressive optical imaging within the Rytov approximation," *Optics Letters*, vol. 37, no. 10, pp. 1760-1762, 2012.

[16] G. Oliveri, P. Rocca, and A. Massa, "A Bayesian compressive sampling-based inversion for imaging sparse scatterers," *IEEE Trans. Geosci. Remote Sens.*, vol. 49, no. 10, pp. 3993-4006, Oct. 2011.

[17] G. Oliveri, M. Salucci, and N. Anselmi, "Tomographic imaging of sparse low-contrast targets in harsh environments through matrix completion," *IEEE Trans. Microw. Theory Tech.*, vol. 66, no. 6, pp. 2714-2730, Jun. 2018.

[18] M. Salucci, A. Gelmini, L. Poli, G. Oliveri, and A. Massa, "Progressive compressive sensing for exploiting frequency-diversity in GPR imaging," *Journal of Electromagnetic Waves and Applications*, vol. 32, no. 9, pp. 1164- 1193, 2018.